DOI: 10.1002/jemt.22078

Harmonic Optical Microscopy and Fluorescence Lifetime Imaging Platform for Multimodal Imaging

VITOR B. PELEGATI,[1,2] JAVIER ADUR,[1,2]* ANDRÉ A. DE THOMAZ,[1] DIOGO B. ALMEIDA,[1] MARIANA O. BARATTI,[1] LILIANA A. L. A. ANDRADE,[3] FÁTIMA. BOTTCHER-LUIZ,[4] AND CARLOS. L. CESAR[1]

[1]*Biomedical Lasers Application Laboratory. Optics and Photonics Research Center, "Gleb Wataghin" Institute of Physics. State University of Campinas (UNICAMP). Departamento de Eletrônica Quôntica. Rua Sergio Buarque de Holanda, 777. Cidade Universitária "Zeferino Vaz". Campinas 13083-859. São Paulo. Brazil*

[2]*Microscopy Laboratory Applied to Molecular and Cellular Studies. School of Bioengineering. National University of Entre Ríos (UNER). Ruta 11, km 10, Oro Verde 3101. Entre Ríos. Argentina*

[3]*Department of Pathology. State University of Campinas (UNICAMP). Faculdade de Ciências Médicas, Departamento de Anatomia Patológica. Cidade Universitária "Zeferino Vaz". Campinas 13083-970. São Paulo. Brazil*

[4]*Department of Obstetrics and Gynecology. State University of Campinas (UNICAMP). Faculdade de Ciências Médicas, Departamento de Tocoginecologia. Cidade Universitária "Zeferino Vaz". CAISM. Laboratœrio de Citogenética e Cultivo Celular. 13083-970 Campinas. São Paulo. Brazil*

KEY WORDS two-photon excitation fluorescence; second and third harmonic generation; fluorescence lifetime

ABSTRACT In this work, we proposed and built a multimodal optical setup that extends a commercially available confocal microscope (Olympus VF300) to include nonlinear second harmonic generation (SHG) and third harmonic generation (THG) optical (NLO) microscopy and fluorescence lifetime imaging microscopy (FLIM). We explored all the flexibility offered by this commercial confocal microscope to include the nonlinear microscopy capabilities. The setup allows image acquisition with confocal, brightfield, NLO/multiphoton and FLIM imaging. Simultaneously, two-photon excited fluorescence (TPEF) and SHG are well established in the biomedical imaging area, because one can use the same ultrafast laser and detectors set to acquire both signals simultaneously. Because the integration with FLIM requires a separated modulus, there are fewer reports of TPEF+SHG+FLIM in the literature. The lack of reports of a TPEF+SHG+THG+FLIM system is mainly due to difficulties with THG because the present NLO laser sources generate THG in an UV wavelength range incompatible with microscope optics. In this article, we report the development of an easy-to-operate platform capable to perform two-photon fluorescence (TPFE), SHG, THG, and FLIM using a single 80 MHz femtosecond Ti:sapphire laser source. We described the modifications over the confocal system necessary to implement this integration and verified the presence of SHG and THG signals by several physical evidences. Finally, we demonstrated the use of this integrated system by acquiring images of vegetables and epithelial cancer biological samples. *Microsc. Res. Tech. 75:1383–1394, 2012.*

INTRODUCTION

Nonlinear optical (NLO) microscopy evolved as an alternative to conventional single-photon confocal microscopy and has been shown to provide several advantages. These include 3D resolved fluorescence imaging of living cells deep within thick, strongly scattering samples, and reduced phototoxicity, enabling long-term imaging (Diaspro, 2011). NLO signals depend on the probability of finding more than one photon in space and time, which is dramatically enhanced at the focus of a pulsed femtosecond laser. Moreover, the light pulse repetition is a natural clock to perform fluorescence lifetime imaging microscopy (FLIM). These nondestructive techniques have the potential to offer new insights into complex developmental processes of many biological settings. Two-photon excited fluorescence (TPEF) provides functional information of molecules, while second harmonic generation (SHG) and third harmonic generation (THG) microscopy can be used to image organized biological extracellular and subcellular structures and interfaces (Chu et al., 2001). Furthermore, FLIM is sensitive to the chemical microenvironment around the fluorophores such as pH, ion, and oxygen concentration (Bird et al., 2004; Provenzano et al., 2009).

Any single modality typically only furnishes an incomplete picture of the tissue; hence, an approach that integrates complementary optical imaging modalities is needed for a more comprehensive nondestruc-

*V.B.P. and J.A. contributed equally to this work.

*Correspondence to: Javier Adur, National University of Entre Ríos, Departamento Biología, Ruta 11 Km10, Oro Verde 3101, Entre Ríos Argentina. E-mail: jadur@bioingenieria.edu.ar

Received 22 December 2011; accepted in revised form 28 April 2012

Contract grant sponsors: CEPOF (the Optics and Photonics Research Center, FAPESP); National Institute of Photonics Applied to Cell Biology (INFABIC).

DOI 10.1002/jemt.22078

Published online 31 May 2012 in Wiley Online Library (wileyonlinelibrary.com).

tive and minimally invasive tissue characterization. Integration of the various techniques is one of the evolving areas in bioimaging. Different modalities of NLO microscopy have been developed and combined for imaging complex tissue samples with inherent 3D spatial resolution.

Two-photon fluorescence (TPFE) microscopy first appeared in the 1990 (Denk et al., 1990) using a laser scanning Bio-Rad microscope and a femtosecond colliding pulse mode (CPM) dye laser. Non-scanning SHG microscopy can be traced back to Hellwarth and Christensen in 1975 (Hellwarth and Christensen, 1975). In 1978, Gannaway and Sheppard used a sample scanning microscope to acquire images of inorganic crystals (Gannaway and Sheppard, 1978). The first biological image was acquired by Freund in 1986 (Freund et al., 1986), still by scanning the sample and not the laser, who observed the orientation of collagen fibers in rat-tail tendon. In the late 90s, Alfano's group published a sequence of articles showing TPEF, SHG, and THG on biological samples. They started with a CPM dye laser and evolved to Ti:sapphire laser, performing the spectroscopic studies to show that the signals were indeed due to the harmonic generation. In terms of imaging, they used a sample scanning to acquire a tomography (y vs z) image of chicken tissue and even different kinds of tumors (Alfano et al., 2001; Guo et al., 1996, 1997a, 1997b, 1998, 1999). The quality of confocal images has been always related to the scanning method, laser or sample scanning. Only after Amos and White developed a laser scanning system in 1987 (Amos and White, 2003) a successful commercial system appeared, the Bio-Rad MRC 500. To our knowledge, the first laser scanning high-resolution SHG image was obtained in 1999 by Campagnola who observed TPEF and SHG of several biological samples (Campagnola et al., 1999). THG tomography (x vs z) of optical fiber glasses was observed in 1997 (Barad et al., 1997). Squier et al. showed a laser scanning image of biological materials in 1998 (Squier et al., 1998). Chu et al. then showed a multimodal imaging including TPEF+SHG+THG in 2001 (Chu et al., 2001).

FLIM was observed in laser scanning system in 1989 (Bugiel et al., 1989) and combined with TPFE in 1996 (König et al., 1996; Yu et al., 1996). Since then, it became clear that FLIM is a technique that can be integrated with all different NLO microscopies providing important information about the molecules chemical environment (Zoumi et al., 2002).

The most common commercial excitation source for nonlinear microscopy is the Ti:sapphire laser with femtosecond pulses, average output power of several watts, repetition rate around 80 MHz, and a tuning wavelength range approximately between 690 and 1,040 nm. For THG microscopy, however, the THG signal is generated in the 230–350-nm UV wavelength range where there is a strong absorption, which limits its application to thin biological specimens. Moreover, the commercial microscope optics, coatings and transmission, are usually not adequate for this UV region. To avoid these problems, several groups are using laser sources with wavelengths longer than 1,200 nm. Cr:Forsterite laser at excitation wavelength of 1,230 nm and repetition rate of 110 MHz is widely used (Chan et al., 2008; Chu et al., 2001). Other lasers include optical parametric oscillators (OPO) working at the wavelength of 1,500 nm and repetition rate of ~80 MHz (Canioni et al., 2001); optical parametric amplifiers at 1,200 nm and 250 kHz repetition rate pumped by a Ti:sapphire laser (Squier et al., 1998); and fiber lasers at 1,560 nm with repetition rate of 50 MHz (Millard et al., 1999). Some new laser sources being used for nonlinear microscopy are Yb:glass, Nd:glass, Cr:LiSAF, and fiber lasers. However, these laser sources are expensive and difficult to use.

Recently, a multimodal microscopic technique was implemented by a combination of THG, SHG, and MPEF image contrast methods on the same microscope (Gualda et al., 2008). Similarly, in the last year, we built a multimodal microscopic combining TPFE, SHG, and THG in the same platform (Adur et al., 2011). Other important reports on confocal setups modified for harmonic generation could be find at (Carriles et al., 2009; Cox et al., 2005; Sun, 2005; Sun et al., 2004). However, these home built systems lack the FLIM modality.

In this work, we show how to build a nonlinear/multiphoton microscope on a commercial confocal system platform (inverted Olympus IX81 with FV300 scan head), easy-to-operate, capable to perform TPFE, SHG, THG, and FLIM imaging, using only the standard femtosecond Ti:sapphire laser. To our knowledge, this is the first report of a multimodal system including TPEF+SHG+THG+FLIM. We demonstrated that it is possible to obtain good THG signal, even for thick biological samples, with excitation wavelength below 1,000 nm. We show the modifications over the scan head and the detector we made to acquire THG signals, present the physical evidences of the higher harmonics presence and applied this multimodal system to acquire images of plant samples and ovarian cancer tissues.

MATERIALS AND METHODS

Construction of a Multimodal Nonlinear Optical Imaging Platform

In this section, we provide details of our multimodal workstation, including the excitation source, confocal microscope and the implementation of the backward and forward detection systems.

The Excitation Source and Confocal Microscope. The schematic of the setup is shown in Figure 1. The femtosecond laser is a Ti:Sapphire Mai Tai high-pass (HP) spectra-physics (Irvine), which provides $<$100 fs pulses from 690 to 1,040 nm with 80-MHz repetition rate and output power from 1 to 3.5 W. It was equipped with a DeepSee for group-velocity dispersion compensation and a broadband half-wave plate, coupled to a calcite polarizing beam splitter, as an attenuator. The beam is coupled to the scan head through a custom made port and a dichroic mirror. A collimating telescope (L1, L2) is used to adjust both the beam diameter to fill the objective back-aperture of the PLANAPO 40× high numerical aperture (NA) (1.3 NA) oil immersion objective and the beam focus position on the microscope focal plane.

An Olympus FV300 scanner and the laser combiner FV-5 COMB 2 by Olympus (Olympus, Tokyo, Japan) system built onto an Olympus inverted research microscope IX-81 is used in the setup. The FV300 scanner unit has two input ports, one for a continuous wave

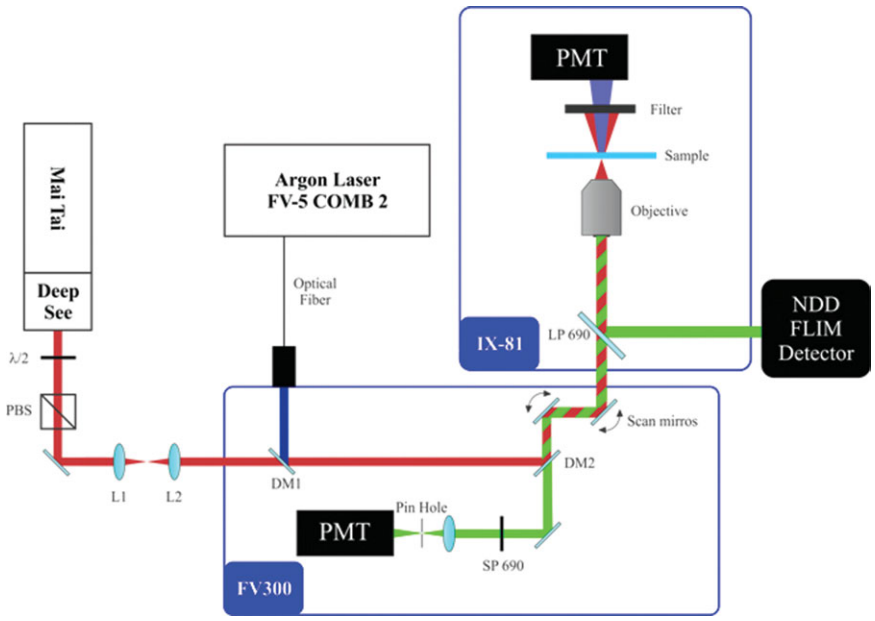

Fig. 1. Schematic diagram of a multimodal NLO microscope using a femtosecond laser source. The Mai Tai output at 940 nm is couple to the FV300 confocal scanning head and inverted microscope Olympus IX-81 (Olympus, Japan). The 940-nm beam is used for TPEF, SHG, and THG imaging. The signal beam at 890 nm is used also for TPEF and FLIM imaging. One internal PMT detector is used for TPEF backward analysis and other PMT external detectors is added for forward SHG and THG detection. Backward FLIM signal is detected in NDD way with B&H detector. λ/2, half wave plate; PBS, polarizing beam splitter; L1-L2, telescope lens; DM1 and DM2, dichroic mirrors; SP, short pass filter; LP, long past filter. [Color figure can be viewed in the online issue, which is available at wileyonlinelibrary.com.]

(CW) laser, and the other specifically designed for the pulsed Ti:Sapphire laser. The other components in the excitation pathway are dichroic mirror to couple both, CW and pulsed lasers, excitation dichroic mirror, XY galvanometer mirror scanners, and pupil lens. The excitation for confocal microscopy is provided by an Argon ion laser. Light from the laser source is brought into the scan head using an optical fiber cable. The inverted IX-81 microscope used in the setup is a fully motorized advanced research microscope, which provides halogen lamp as well as epifluorescent imaging using an epifluorescent attachment and UV lamp. Standard differential interference contrast (DIC) microscopy could also be obtained simultaneously with confocal imaging.

The system offers standard three-channel detection, two internal (inside of scan head), and one external, for transmitted light imaging. The epidetected fluorescence light is collected with the objective, descanned at the galvo-mirrors, separated from the excitation by a dichroic emission beam splitter, and focused on the pinhole with a collector lens. Our pinhole turret has 60, 100, 150, 200, and 300 μm confocal apertures. A dichroic filter after the pinhole allows the selection of two wavelength windows, each one with a barrier filter in front of the internal photomultiplier detector to completely block the laser. The microscope back ports and two side ports were used for harmonic and FLIM detection.

Detection of Nonlinear Signals. NLO images were acquired with the 940 nm excitation, generating a TPFE above 500 nm, SHG at 470 nm and THG at 313 nm. For this work, FLIM data were acquired with the 890 nm excitation, which excites mainly the fluorescence of flavin adenine dinucleotide (FAD) (Skala et al., 2007).

TPEF and FLIM signals were detected in backward configuration. In particular, the TPEF signal was descanned detected with the internal scan head photomultiplier tubes (PMT) [R3896 PMTs; Hamamatsu Photonics, Hamamatsu City, Japan] after a blocking filter (SP) E-700-SP (Omega Filters) to prevent back-reflected laser light with a completely open pinhole. FLIM signal was non-descanned detected using an internal dichroic beamsplitter and one side port of the IX-81 microscope. Data were collected pixel by pixel with a fast photon-counting PMT detector (Becker & Hickl, PMH-100) and time correlated single photon-counting electronics (Becker & Hickl, SPC-830), after a HP filter (E-690-HP, Omega Filters). This non-descanned FLIM detector is equipped with overload shutdown and electronically controlled shutters to minimize the risk of detector damage. The shutter assembly also contains the lens that transfers the photons to the detector. FLIM and TPEF can be acquired simultaneously.

SHG and THG signals were collected in forward direction using an external detector. THG UV signal is generated at the sample, but it can be absorbed by optical elements in the beam pathway. To avoid this, we decided to place the detector right after the sample. For that, we replaced the microscope condenser with a special homemade PMT support and hold it as close to the sample as possible, without touching it, but with enough space for the optical filters (Fig. 2, top photographs). The PMT large area assured a good NA collection angle. To detect SHG signal, we used an E700-SP short pass-filter followed by a narrow (10 nm full width

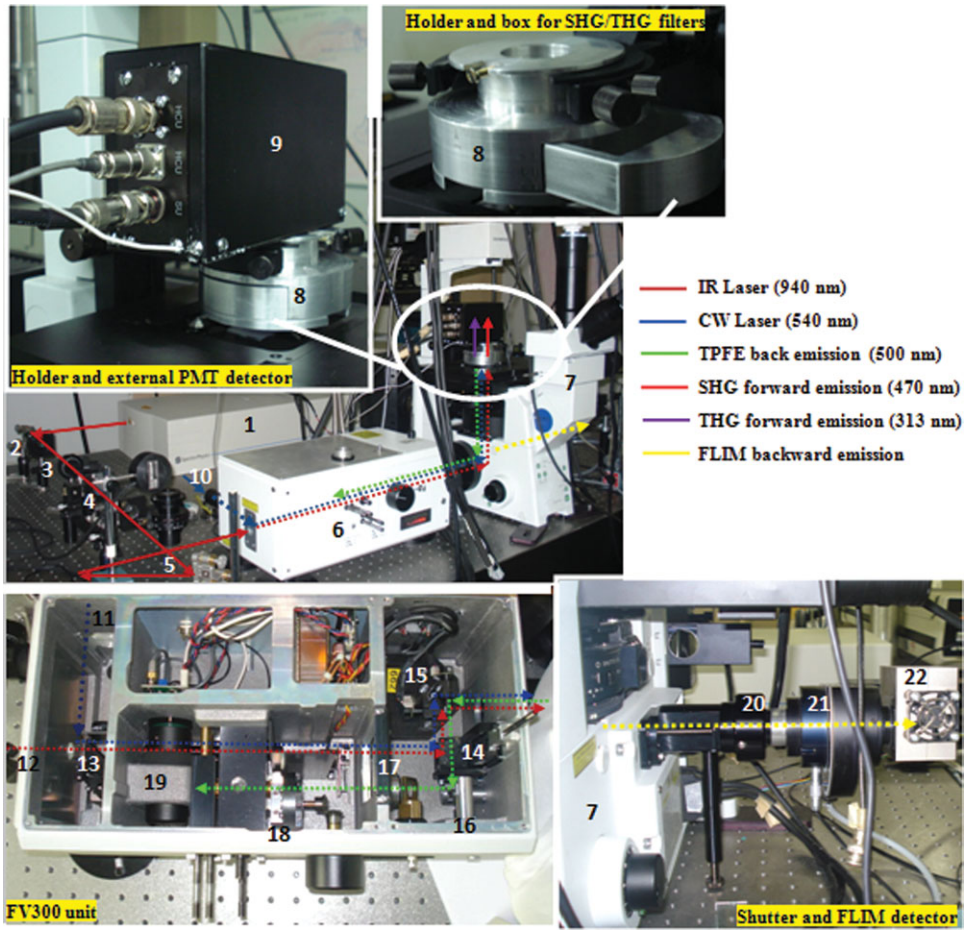

Fig. 2. Real setup showing in the center: laser way and Olympus FV300 confocal scanning head coupled to the inverted microscope Olympus IX-8, in the top: external PMT and special holder and in the bottom: internal vision of scan head and FLIM setup detection. 1: Mai Tai laser and DeepSee module, 2: reflected IR mirror, 3: half wave plate and polarizing beam splitter, 4: telescope, 5: reflected IR mirror, 6: scan head 7: inverted microscopy, 8: holder and box filters, 9: external PMT, 10: Argon laser, 11: input port to Argon laser, 12: input port to Mai Tai, 13 and 14: dichroic mirrors, 15: galvanometer mirror scanners, 16: collector lens, 17: short pass filter, 18: pinhole, 19: internal PMT, 20: FLIM NDD port, 21: shutter and 22: photon-counting PMT detector. [Color figure can be viewed in the online issue, which is available at wileyonlinelibrary.com.]

at half maximum (FWHM)) bandpass optical filter centered at half the excitation wavelength (475BP, Bio-Rad) to reject the excitation laser beam and any unwanted fluorescence. To collect THG images, we replaced both SHG filters with two colored glass filters U340 ± 30 nm (Hoya Corporation). SHG and THG images were acquired one after the other due to the exchange of the optical filters, but simultaneously with the TPEF images. Both TPEF were compared to make sure that the sample did not move during the optical filter exchange procedure. Except for this exchange of filters, the system is very friendly to use.

A complete illustration of the different light paths, filters, dichroic mirrors, and detectors distributions that compose this multimodal system can be found in Figure 2. Blue and dark red lines indicate CW Argon laser and pulsed near infrared (NIR) excitation light directed onto the sample for confocal and NLO modality, respectively. Green lines indicate fluorescence emission light from confocal and epifluorescence modes. Red and blue lines indicate forward propagating SHG and THG signal, respectively, while yellow lines indicate the backward propagating FLIM signal.

Acquisition and Analysis. All TPFE, SHG, and THG images were acquired with 512 × 512 pixel spatial resolution, using 5ms for the pixel dwell time, with total scanning time of the order of 3 s, after a five-frames Kalman filtering. Images (pseudogreen TPEF, pseudored SHG, and pseudomagenta THG) were combined into a single image for visualization using Olympus Fluoview Image Browser. For visual presentation, images were optimized by background thresholding and histogram stretching. Although these techniques improved visual image contrast and presentation, all image analyses processed with ImageJ (NIH, available from http://rsb.info.nih.gov/ij) were performed on the unprocessed images to avoid any artifacts. FLIM data were collected for 60 s with a 256 × 256-pixel frame size. The imaging program (SPCImage Ver. 2.9, Becker & Hickl) determines the best exponential fit to the histograms at each pixel and displays lifetime data utilizing a color-mapping scheme.

Sample Preparation

For the illustration of the workstation capabilities, we utilized different biological samples. For a quick and easy evaluation of our system, we first worked with vegetables and used fresh *Solanum tuberosum* (potato) and *Allium cepa* (onion samples). Using a scalpel, thick sections (≈300 μm) were obtained for tridimensional reconstruction. Finally, to demonstrate the utility of this multimodal system, we work with human biopsies and recognized differences between various subtypes of mucinous ovarian tumor. These biopsies were obtained from women attending at Women's Health Center CAISM, Campinas, SP, Brazil, and the project was approved by the Institutional Ethics Committee (Faculty of Medical Sciences, Unicamp). Ovarian specimens collected during surgical procedures were prepared following a standard histological procedure: fixed in 10% buffered formalin, embedded in paraffin, cut in 4-μm thick sections and mounted on slides. Slides from serial sections were stained with H&E and covered with coverslips. We also used unstained slides to perform FLIM analysis. Each H&E stained tissue section was evaluated by a certified pathologist, based on established World Health Organization histological criteria.

RESULTS AND DISCUSSION

Characteristics and Contrast Mechanism of the Implemented Techniques

TPEF is a third-order NLO resonant process where two photons excite an electron from the ground state. It is an inelastic process where photon energy is released at the sample. Two-photon absorption happens only when the energy of the incident photons fall into the two-photon excitation band which is specific for each fluorescent marker. The two-photon excitation band is not exactly half of the one photon excitation band because the selection rules are different. The fact that two-photon excitation (TPE) depends on the square of the incident light provides its confocal characteristics, that is, a process happening only at a focal point volume. On the other hand, the emission after the excitation is an incoherent optical process with a lifetime that depends not only on the excited molecule, but on the chemical environment around it. Photobleaching is smaller in TPFE compared to single photon excitation because the excited volume is smaller. Therefore, TPEF allow the observation of specific markers, by choosing both, the excitation and emission wavelength, as well as by observing different fluorescence lifetimes.

SHG and THG, on the other hand, are coherent second/third-order elastic NLO processes. Because two/three photons generate another photon with two/three times the energy of the incident photons, there is no energy released to the medium, meaning no infocus cell photodamages are expected from these processes, although there is always a damage threshold intensity, or fluence, for ultrafast laser pulses due to multiphoton ionization. Both SHG/THG can be isolated from fluorescence by the wavelength or even by time gating, because the coherent processes are practically instantaneously. The fact that SHG signal is proportional to I^2 while THG signal is proportional to I^3, where I is the incident light intensity, which provides confocality for both techniques. For the same wavelength of the incident light, THG has better optical sectioning resolution than SHG. One practical problem with THG is the fact that its wavelength range in the UV-blue part of the spectrum tends to become resonant with molecule's electron level transitions, with higher absorption. Besides, scattering also increases in the UV-blue range. (Carriles et al., 2009).

Usually, the third-order nonlinear susceptibility (χ^3), responsible for THG, is much smaller than the second-order nonlinear susceptibility (χ^2), responsible for SHG. In principle, this would mean that THG should be much harder to observe. However, χ^2, as well as any other even susceptibilities coefficients, must be null in the presence of inversion symmetry. Therefore, SHG shall be zero in the presence of centrosymmetric molecules, unless an external parameter, such as electric fields or interfaces, breaks the symmetry. On the other hand, all materials have nonzero third-order susceptibility χ^3. Moreover, χ^3 can be several orders of magnitude larger or smaller for different materials. Compared to only a fractional difference ~20% of the refractive indexes, (χ^1) of most materials, this would mean a much higher contrast than phase contrast or DIC microscopy. However, THG is null in a homogeneous material, no matter how high χ^3 could be, because the Gouy-phase shift of π across the focus of a Gaussian excitation beam creates a destructive interference between signals generated before and after the focus (Boyd, 1992). However, for a nonhomogeneous focal volume a measurable amount of THG is generated (Debarre and Beaurepaire, 2007). Because heterogeneity is more common in biology than homogeneity, THG provides an important tool for bioimaging, with the warning that it tends to be brighter at the interface of large granules, droplets or other biostructures compared to the internal signal.

SHG imaging modality can probe molecular organization on the microscale as well as the nanoscale. SHG cancellation occurs whenever emitters are aligned in opposing directions within the focal volume of the laser. Such situation occurs in isotropic media and media with cubic symmetry. Nonlinear emission dipoles aligned in an antiparallel arrangement produce SHG exactly out of phase; and hence, the signals cancel due to destructive interference. Selective SHG cancellation due to central symmetry has recently been observed in several biologically relevant systems including lipid vesicles infused with styryl dye, anisotropic bands in muscle cells, and plant starch granules (Moreaux et al., 2000; Prent et al., 2008). In biological materials where SHG emitters are well organized in noncentrosymmetric microcrystalline structures, the SHG from different emitters adds coherently resulting in very intense SHG. Some examples of such structures include the starch granules, other polysaccharides, collagen, striated muscle, and chloroplasts (Campagnola and Yuan-Dong, 2011; Chu et al., 2001).

THG have been used to monitor embryo development and mitosis in zebra fish (Chu et al., 2003; Sun et al., 2004), to observe human glial cells (Barille et al., 2001), cardiomyocites (Barzda et al., 2005), green algae rhizoids (Squier et al., 1998), chloroplasts (Muller et al., 1998), erythrocytes (Millard et al., 1999), epithelial, neuron, and muscle cells (Yelin et al., 2002), and

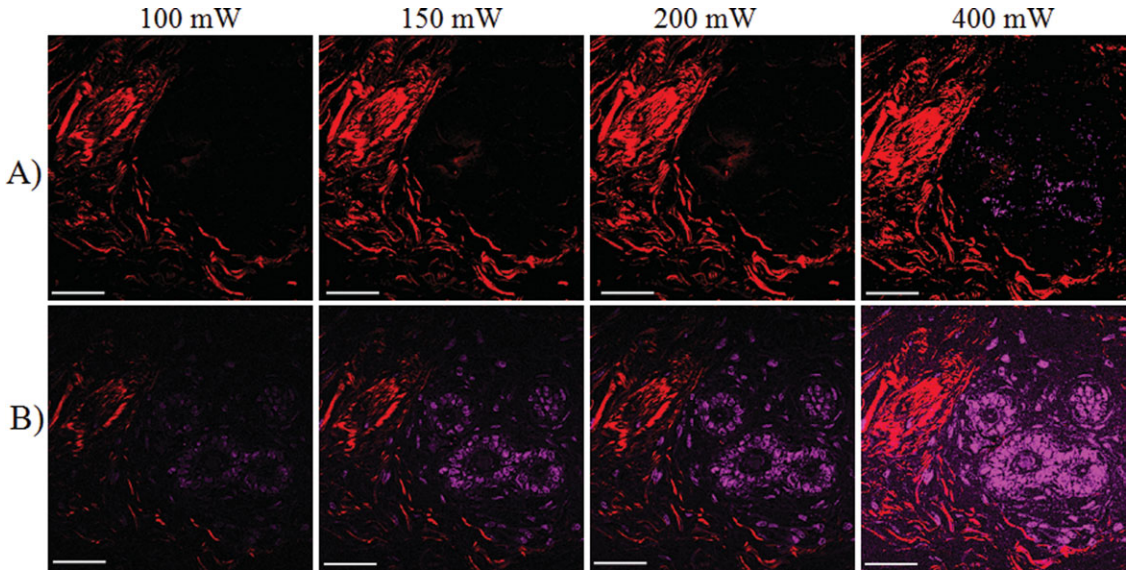

Fig. 3. Representative SHG and THG images from a thin section (~5 μm) of normal human breast sample stained with H&E. The signals were obtained using different setup (**A**) with condenser lens and (**B**) without condenser lens. All images were captured with same gain of PMT and varying the power laser between 100 and 400 mW. THG was difficult to detect (setup A) due to poor UV transmission of the condenser lens. Scale bar = 50 μm. [Color figure can be viewed in the online issue, which is available at wileyonlinelibrary.com.]

Ca^{2+} intracellular dynamics (Canioni et al., 2001). Our experience with both techniques using the system described in this article to study cancer tumors is that SHG is excellent to observe collagen network of extracellular tissue, whereas THG can display clearly the nuclei, two very important information for pathologists (Adur et al., 2011).

Characterization of SHG and THG Signal

We first evaluate the ability of our system to detect SHG and THG signal using a wavelength of the excitation below 1,000 nm. We used 940 nm in this work generating a SHG signal at 470 nm (visible) and a THG signal at 313 nm (ultraviolet), respectively. To collect transmitted SHG and THG simultaneously, we would need to use a high NA (Cox et al., 2005; Millard et al., 2003) condenser to collect both signal and then split them with a dichroic to two PMTs. The condenser shall have a NA similar or higher than the objective lens to achieve optimal collection of the signals and also a good transmission curve in UV region (Carriles et al., 2009). However, our specific condenser had neither the right NA nor the good UV transmission, probably due to the lenses optical coatings. Therefore, we decided to simply remove the condenser and place the PMT as close as possible to the sample to increase the collection angle. Figure 3 shows a comparison of SHG and THG signal generated by a fixed breast tissue sample collected with (row A) and without (row B) the condenser. For all laser powers tested (100–400 mW), good SHG (red) and THG (magenta) signal were detected using the PMT directly over the sample (without condenser lens, row B) but only good SHG signal was detected using the condenser (row A). A weak THG signal was detected only at the highest power (400 mW, row A) with the condenser. At this laser power without the condenser (row b), the SHG signal was saturated and the sample was damaged after sometime. The main problem with the condenser was the poor UV transmission, because its collection NA was better than the collection NA of the PMT directly over the sample. We, therefore, demonstrated that removing the condenser lens and using a special support for an external PMT (Fig. 2, top photographs), it is possible to get good THG signal from a femtosecond Ti:sapphire laser. However, in this geometry, it was impossible to collect both, transmitted SHG and THG, simultaneously.

We also tested the THG contrast to local heterogeneities of size smaller or comparable to the beam focus (Debarre and Beaurepaire, 2007). To do that we analyzed the THG generated by the 940-nm laser beam in the air-glass interface shown in Figure 4 where the Mai Tai laser was focused with a lens into a coverslip positioned in a translation stage. The resultant emission was registered using a monochromator/charge-coupled device (CCD) system (Acton Research modelo Spectra-Pro 300i/CCD "back-illuminated" Princeton Instruments). THG signal only appeared, visible to a naked eye, when the laser was focused at the air-glass interface. It disappeared when we removed the lens but not the 940 nm excitation, which was also detected by the CCD. We varied the laser power from 430 to 1,140 mW, measured before the lens, and performed the same measurements shown in Figure 4A for different laser intensities. Figure 4B (black plot) shows the result of the wavelength integrated THG signal versus laser power in a log-log plot, which presented the expected THG signal proportional to the cube of the laser intensity. We then performed a similar experiment directly in the microscope setup shown in Figure 1 by placing a coverslip (170 μm thickness) in the objective focus and acquiring several scanning images at different depths (Fig. 4C). The THG intensity was obtained with the Olympus Fluoview software. Figure

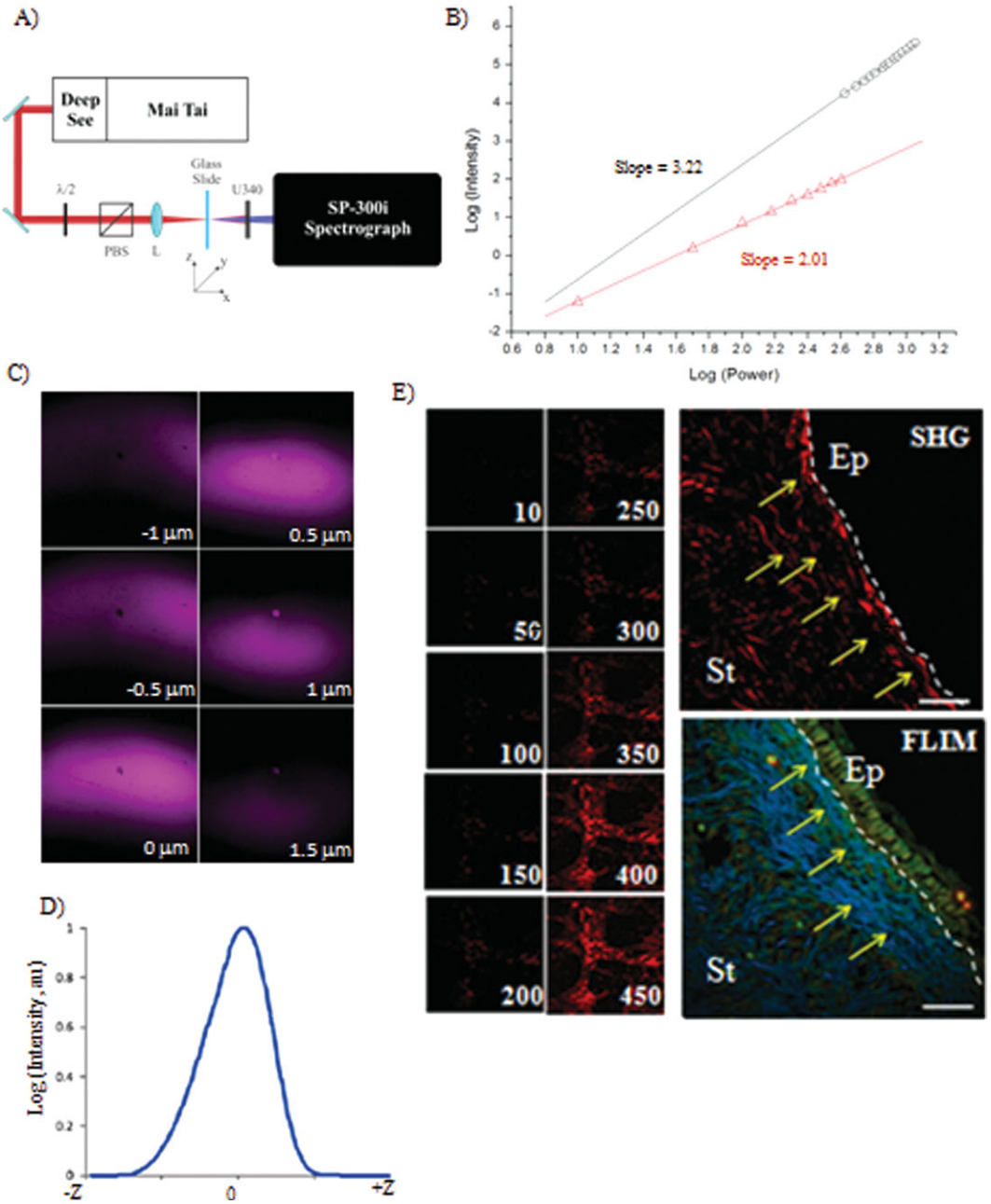

Fig. 4. THG and SHG characterizations. **A**: Schematic setup used to analyze the THG generated in the air-glass interface. **B**: Log–log graph of THG intensity (black plot) and SHG intensity (red plot) for laser output power. The circles and triangles are experimental data and the solid lines are lines with slopes near to 2 (red) and 3 (black), respectively. **C**: Several THG images at different depth of glass-air interface of coverslip. **D**: TGH intensity of signal shows in C, the maximum is obtained when the interface are in focal position. **E**: In the left, images used to perform log–log graph of SHG intensity (B), obtained at the different excitation power conditions (10–450 mW). The specimens are serial sections of fixed stained-H&E and unstained piece of a human ovary excited at 940 nm. In the right, SHG and FLIM images of ovarian stroma excited at 890 nm. Collagen fibers (yellow arrows) show very fast lifetime components (blue color) comparative to auto fluorescence of epithelial cells (yellow/green color). λ/2, half wave plate; PBS, polarizing beam splitter; L, lens; U340, THG filter; St, stroma; Ep, epithelium; epithelial/stromal interface is indicated (white outline). Scale bar = 20 µm. [Color figure can be viewed in the online issue, which is available at wileyonlinelibrary.com.]

4D shows the plot of the THG intensity vs focal position, which presents a peak at the focal position and disappeared after ~1 µm dislocation for each side. Next, we exchanged the filters to detect the SHG signal from ovary tissues specimen, which has rich collagen content in the stroma (Kirkpatrick et al., 2007), a protein well known as a good source of SHG signal (Campagnola and Yuan-Dong, 2011). Using this sample, we performed two experiments. First, we measured the SHG intensity as a function of laser power varying

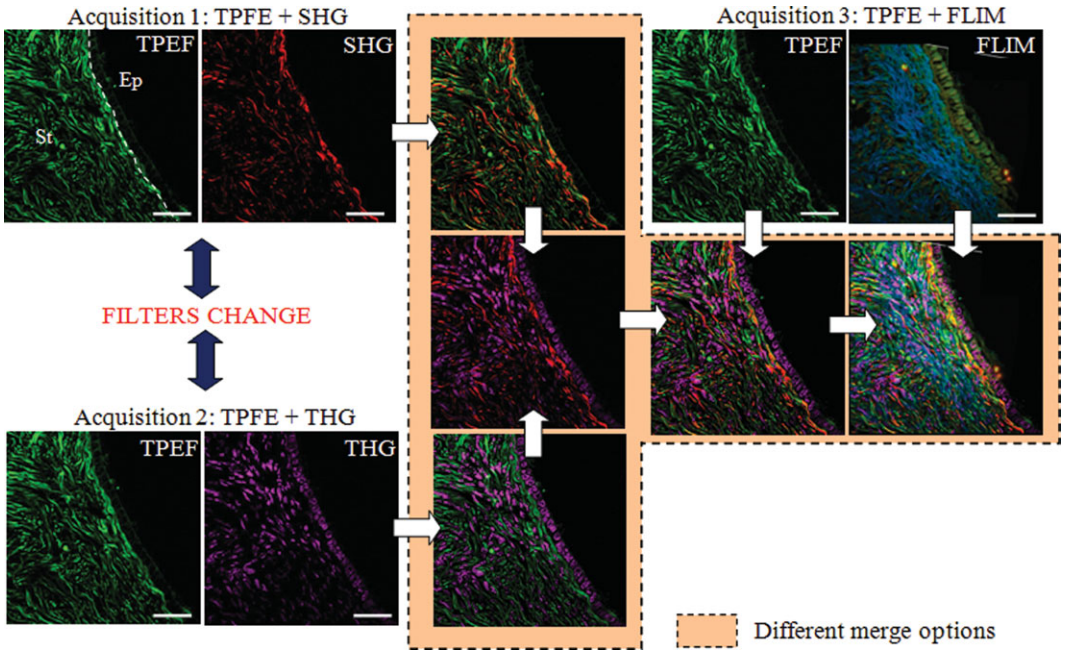

Fig. 5. Representative NLO images from a thin section (~5 μm) of normal human ovary sample stained with H&E. Different acquisition modes and possibilities of combination using NLO microscopy platform are presented. SHG (red), THG (magenta), and FLIM (blue/yellow/green) images were obtained simultaneity with TPEF (green) images. Superimposition of each modality is show inside orange shading rectangle. St, stroma; Ep, epithelium; epithelial/stromal interface is indicated (white outline). Scale bars = 20 μm. [Color figure can be viewed in the online issue, which is available at wileyonlinelibrary.com.]

from 10 to 450 mW (Fig. 4E) and checked that it was proportional to the second power of the incident light (Fig. 4B, red plot). The intensity value is an average of the whole image and was measured using ImageJ software. Second, we acquired a lifetime (FLIM) image over the same sample and checked that the lifetime was within the instrument response function in the regions correspondent to collagen fibers (Fig. 4E, yellow arrows). Taken all these results together we verified, therefore, that we were actually observing second and THG signal.

Simultaneous Acquisition Signals with TPFE

To demonstrate the system flexibility and easy to use, we show in Figure 5 the different acquisition modes and possibilities of combination into a single image using the Olympus Fluoview Image Browser (Fig. 5, orange shading). We first checked that SHG (red) and THG (magenta) signal are superposed correctly after the exchange of filters. To do this, we use the TPFE (green) signal captured simultaneously with both, SHG and THG, as an image superposition control. This procedure was repeated with FLIM images as well. Figure 5 shows the good correspondences obtained with this setup and that our filter box, careful designed to allow an easy displacement, was working properly. Next, we then proceed to image acquisition of several samples.

Figure 5 shows representative NLO images from a thin section (~5 μm) of normal human ovary sample stained with H&E. Recent reports (Adur et al., 2011; Tuer et al., 2010;) showed that H&E traditional staining method is not only useful to generate TPFE signal but that it also enhanced the THG signal without any harm to the SHG signal. We can see that TPEF signal corresponding to eosin fluorescence was strong outside the nuclei but weak in the nuclear regions. The SHG corresponds to collagen within the stromal connective tissue and the THG signal strongly highlights the nuclei. The FLIM images provide more information and allow the correlation of the lifetime to these different structures. These results agree with the literature (Nadiarnykh et al., 2010; Williams et al., 2010) and shows that the structural information revealed by each nonlinear contrast mechanism can be isolated and analyzed separately with this system, while their superimposition allows a better comparison and understanding of the spatial organization of the tissue.

SHG and THG Microscopes in Thick Samples

After checking that SHG and THG can be superimposed correctly, we demonstrated that our system can also work with thick unstained fresh samples. Figure 6 shows maximum projection images of *Allium cepa* (onion, Fig. 6A) and *Solanum tuberosum* (potato, Fig. 6B) samples. Approximately, between 50- and 300-μm thick sections were immediately analyzed after removal. Final SHG and THG images superposition are presented. The superposition of SHG and THG images in potato do not correlate well probably due to tissue dehydration that happened between the image acquisition and filter exchange, resulting in a deformation of the structures. In onion samples, elongated and oval big cells are observed by the harmonic signal originated at the interface of secondary cell wall (Mizutani et al., 2000). The nucleus is observed principally by

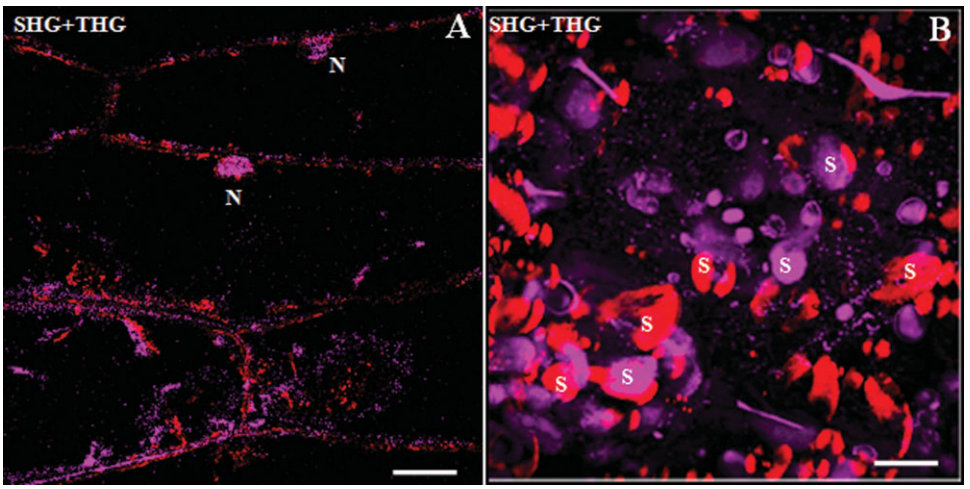

Fig. 6. Simultaneous multimodal SHG and THG tridimensional imaging of fresh samples of *Allium cepa* "onion" (**A**) and *Solanum tuberosum* "potato" (**B**). Maximum projection of 10 images obtained each 5 μm (A) and 60 images obtained each 5 μm (B), respectively. N, nucleus; S, starch granules. Scale bar = 50 μm. [Color figure can be viewed in the online issue, which is available at wileyonlinelibrary.com.]

THG signal due to interface of biological membrane (Debarre and Beaurepaire, 2007). On the other hand, the rich SHG/THG contrast source in potato must come from starch granules, droplets of lipid and water. It is known that starch granules exhibit high SHG conversion efficiency. In fact, a piece of potato tuber placed in an unfocused, ultra-fast laser beam, can efficiently generate a bright SHG beam in the forward direction, strong enough to be visible to the naked eye even under ambient room light (Mazza et al., 2008). The same structures generate good THG signal because they have a micrometer-size lipid bodies with high third-order nonlinear susceptibility (Debarre et al., 2006).

These results show that our system provide NLO contrast produced purely from endogenous species for several samples. Besides, the fact that SHG and THG signals arise from an induced polarization rather than absorption, leads to reduced photobleaching and phototoxicity relative to fluorescence methods (including multiphoton). Additionally, because the excitation used is in the near-infrared wavelengths, this setup is well suited to study intact tissue samples, with penetration depths up to 300 μm.

Multimodal NLO Techniques Allow Qualitative Analysis of Ovarian Carcinogenesis

Finally, we demonstrate the utility of this multimodal optical setup in a qualitative study of mucinous ovarian human tumors with various pathologic diagnoses. Figure 7 shows representative SHG and THG images of stained-H&E samples (TPFE is not presented for clarity) and FLIM images of unstained, but fixed, samples. Although one could think that sample processing would destroy the FLIM information about the fluorescent molecules chemical environment, it has been recently demonstrated that biological relevant information can be extracted from FLIM analysis performed on unstained processed samples (Conklin et al., 2009). We used SHG, THG, and FLIM techniques to analyze adenoma (Figs. 7B and 7F), borderline (Figs. 7C and 7G), and adenocarcinoma (Figs. 7D and 7H) ovarian tissues, which were then compared with normal tissue (Figs. 7A and 7E). From the THG+SHG-merged image, epithelial/stromal interface was easily identified (Figs. 7A–7D). In these images, collagen fibers with different orientations and distribution can be clearly identified by the SHG signal (red color) in the stroma region. In normal samples, we found that the collagen was more linearly structured with long, straight fibrils, whereas the collagen of abnormal samples exhibits a loss of fine structure and structural organization. From THG (magenta color), we can qualitatively recognized differences in surface epithelium of each tumor type. In the representative normal sample, the cells were distributed in one layer. On the other hand, mucinous tumor shows cells of varying sizes distributed in multiple layers and containing abundant intracytoplasmic mucin with basal nuclei. Mucinous adenoma show cells also in one or two cell layer and uniform distribution. Unlike normal tissue, in borderline tumor and mucinous adenocarcinoma, the epithelial surface showed cells of varying sizes distributed in multiple layers, including cellular atypia and proliferation. These characteristics are distinguishable in enlarged images of insert. FLIM (Figs. 7E–7H) allows us to use cellular FAD as an endogenous biomarker to visualize cells. FAD is a metabolite known to be autofluorescent. Differences in the fluorescence lifetime of FAD between different epithelial cells are color mapped. Epithelial cells of adenocarcinoma tissues showed a longer fluorescent lifetime compared with normal and benign tissues, allowing epithelial cells of malignant ovary to be easily differentiated from epithelial cells of healthy ovary. These longer lifetime values may be due to the sum of FAD and mucin autofluorescence present in tumor epithelium.

In summary, we demonstrated that based on intrinsic optical contrast obtained for each NLO techniques, we can find qualitative differences between healthy and tumoral ovary. Therefore, these biomarkers could be used as an indicator of early diagnosis. Similar

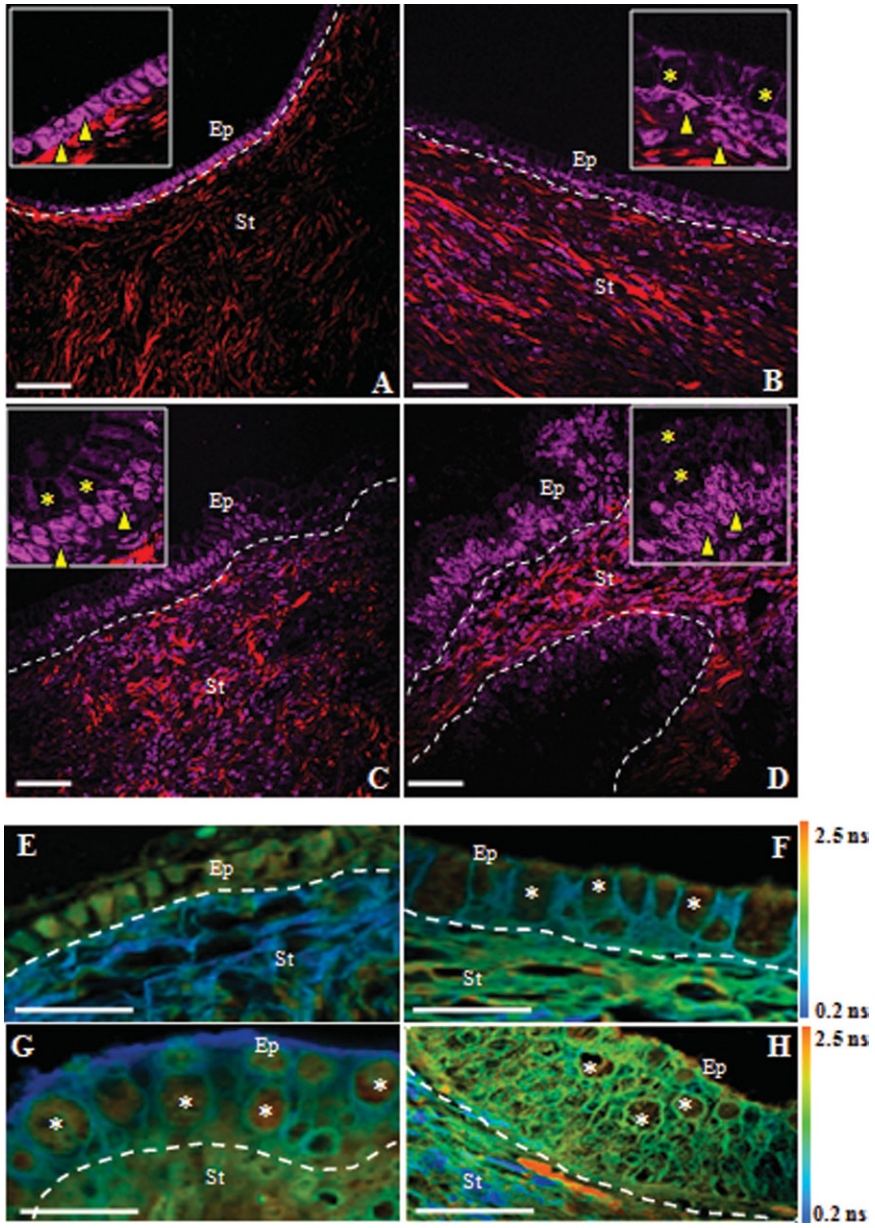

Fig. 7. Representative multimodal images of stained-H&E samples for SHG and THG analyses (**A**–**D**) and unstained samples for FLIM study (**E**–**H**). SHG (red), THG (magenta) and FLIM (blue/yellow/green) images of normal (A, E), adenoma (B, F), borderline (C, G) and adenocarcinoma (D, H) mucinous ovarian human tissues. St, stroma; Ep, epithelium; epithelial/stromal interface is indicated (white outline). Mucin content is indicated with yellow and white asterisk; and epithelial cells are indicated with yellow arrowhead. Scale bars = 20 μm. [Color figure can be viewed in the online issue, which is available at wileyonlinelibrary.com.]

results are shown in the literature using SHG and THG in ovarian tumors from mouse model (Kirkpatrick et al., 2007; Nadiarnykh et al., 2010; Williams et al., 2010). Recently, we quantify these differences in serous ovarian human tumor type (Adur et al., 2011), but this is the first time that FLIM results are presented in human ovarian tumor of this type.

CONCLUSION AND PERSPECTIVES

In this work, we presented a multimodal optical setup that extends a commercially available confocal microscope to include NLO microscopy techniques. We demonstrated that our setup, built on a confocal system platform, is easy-to-operate and can operate with a single standard excitation femtosecond pulse Ti:sapphire laser source. This method provides a cost-efficient way to maximize the bioimaging capabilities of NLO microscopy. Ti:sapphire lasers tuning range in the near IR region, from 690 to 1,040 nm, represents a golden window for tissue imaging, while the femtosecond pulses allow efficient generation of TPEF, SHG, THG and FLIM, signals. We

used this platform to obtain good THG signal in thin and thick fresh biological with 940-nm excitation wavelength.

Although the results presented in this work demonstrate only a small subset of the capabilities of the system, numerous other applications exist in which combined linear and NLO techniques can be important. In this article, we present some practical applications of the developed platform in the field of cancer pathology. Nevertheless, there is a vast field of possible applications that could benefit with the use of this tool. The presented system has great potential for improvements. The first one would be to build a system capable to acquire SHG and THG images simultaneously, by adding a condenser lens with higher NA and UV lenses, and two independent PMTs, avoiding the necessity to exchange filters. Also, OPO lasers can be added to obtain CARS images. The integration of CARS, SHG, THG, FLIM, and multiphoton fluorescence on the same microscope platform will greatly enhance the capability, applicability, and versatility of NLO microscopy.

In summary, the multimodal workstation described here offers a highly flexible, versatile, and complete solution, providing an extremely useful tool of investigation in biology by a simultaneous use of a combination of linear and NLO techniques. The integration of the various microscopy techniques is one of the evolving areas in bioimaging that promises to have a strong impact on the understanding and early detection of various diseases. In this work, we demonstrate qualitatively that multimodal NLO microscopy successfully visualized characteristic features found in benign and malignant lesions of the human ovary. Distinctive SHG, THG, and FLIM patterns were observed in the epithelial/stromal interface of the adenoma, borderline, and adenocarcinoma samples.

ACKNOWLEDGMENTS

The authors are grateful to FAPESP. This work is also linked with CEPOF (the Optics and Photonics Research Center, FAPESP) and the National Institute of Photonics Applied to Cell Biology (INFABIC).

REFERENCES

Adur J, Pelegati VB, Costa LF, Pietro L, de Thomaz AA, Almeida DB, Bottcher-Luiz F, Andrade LA, Cesar CL. 2011. Recognition of serous ovarian tumors in human samples by multimodal nonlinear optical microscopy. J Biomed Opt 16:096017.

Alfano RR, Guo Y, Liu F, Ho PP. Non-linear optical tomography of turbid media, US Patent#6,208,886 B1, March 27, 2001.

Amos WB, White JC. 2003. How the confocal laser scanning microscope entered biological research. Biol Cell 95:335–342.

Barad Y, Eisenberg H, Horowitz M, Silberberg Y. 1997. Nonlinear scanning laser microscopy by third harmonic generation. Appl Phys Lett 70:922–924.

Barille R, Canioni L, Rivet S, Sarger L, Vacher P, Ducret T. 2001. Visualization of intracellular Ca^{2+} dynamics with simultaneous two-photon-excited fluorescence and third-harmonic generation microscopes. Appl Phys Lett 79:4045–4047.

Barzda V, Greenhalgh C, der Au JA, Elmore S, van Beek J, Squier J. 2005. Visualization of mitochondria in cardiomyocytes by simultaneous harmonic generation and fluorescence microscopy. Opt Express 13:8263–8276.

Bird DK, Eliceiri KW, Fan CH, White JG. 2004. Simultaneous two-photon spectral and lifetime fluorescence microscopy. Appl Opt 43:5173–5182.

Boyd R. 1992. Nonlinear optics,1st edn. New York: Academic Press.

Bugiel I, König K, Wabnitz H. 1989. Investigations of cells by fluorescence laser scanning microscopy with subnanosecond time resolution. Lasers Life Sci 3:47–53.

Campagnola PJ, Wei MD, Lewis A, Loew LM. 1999. High-resolution nonlinear optical imaging of live cells by second harmonic generation. Biophys J 77:3341–3349.

Campagnola1 PJ, Yuan Dong C. 2011. Second harmonic generation microscopy: principles and applications to disease diagnosis. Laser Photon Rev 5:13–26.

Canioni L, Rivet S, Sarger L, Barille R, Vacher P, Voisin P. 2001. Imaging of Ca^{2+} intracellular dynamics with a third-harmonic generation microscope. Opt Lett 26:515–517.

Carriles R, Schafer DN, Sheetz KE, Field JJ, Cisek R, Barzda V, Sylvester AW, Squier JA. 2009. Invited review article: Imaging techniques for harmonic and multiphoton absorption fluorescence microscopy. Rev Sci Instrum 80:081101. Review.

Chan MC, Chu SW, Tseng CH, Wen YC, Chen YH, Su GD, Sun CK. 2008. Cr:Forsterite-laser-based fiber-optic nonlinear endoscope with higher efficiencies. Microsc Res Tech 71:559–563.

Chu SW, Chen IH, Liu TM, Chen PC, Sun CK, Lin BL. 2001. Multimodal nonlinear spectral microscopy based on a femtosecond Cr:forsterite laser. Opt Lett 26:1909–1911.

Chu SW, Chen SY, Tsai TH, Liu TM, Lin CY, Tsai HJ, Sun CK. 2003. In vivo developmental biology study using noninvasive multi-harmonic generation microscopy. Opt Express 11:3093–3099.

Cox G, Moreno N, Feijó J. 2005. Second-harmonic imaging of plant polysaccharides. J Biomed Opt 10:024013.

Conklin MW, Provenzano PP, Eliceiri KW, Sullivan R, Keely PJ. 2009. Fluorescence lifetime imaging of endogenous fluorophores in histopathology sections reveals differences between normal and tumor epithelium in carcinoma in situ of the breast. Cell Biochem Biophys 53:145–157.

Debarre D, Beaurepaire E. 2007. Quantitative characterization of biological liquids for third harmonic generation microscopy. Biophys J 92:603–612.

Debarre D, Supatto W, Pena AM, Fabre A, Tordjmann T, Combettes L, Schanne-Klein MC, Beaurepaire E. 2006. Imaging lipid bodies in cells and tissues using third-harmonic generation microscopy. Nat Meth 3:47–53.

Denk W, Strickler JH, Webb WW. 1990. Two-photon laser scanning fluorescence microscopy. Science 248:73–76.

Diaspro A. 2011. Optical fluorescence microscopy. New York: Springer. 258 p.

Freund I, Deutsch M, Sprecher A. 1986. Connective tissue polarity. Optical second-harmonic microscopy, crossed-beam summation, and small-angle scattering in rat-tail tendon. Biophys J 50:693–712.

Gannaway J, Sheppard CJR. 1978. Second harmonic imaging in the scanning optical microscope. Opt Quant Elec 10:435–439.

Gualda EJ, Filippidis G, Voglis G, Mari M, Fotakis C, Tavernarakis N. 2008. In vivo imaging of cellular structures in Caenorhabditis elegans by combined TPEF, SHG and THG microscopy. J Microsc 229:141–150.

Guo Y, Ho PP, Tirksliunas A, Liu F, Alfano RR. 1996. Optical harmonic generation from animal tissues by the use of picosecond and femtosecond laser pulses. Appl Opt 35:6810–6813.

Guo Y, Wang QZ, Zhadin N, Liu F, Demos S, Calistru D, Tirksliunas A, Katz A, Budansky Y, Ho PP, Alfano RR. 1997a. Two-photon excitation of fluorescence from chicken tissue. Appl Opt 36:968–970.

Guo Y, Ho PP, Savage H, Harris D, Sacks P, Schantz S, Liu F, Zhadin N, Alfano RR. 1997b. Second harmonic tomography of tissues. Opt Lett 22:1323–1325.

Guo Y, Ho PP, Liu F, Wang QZ, Alfano RR. 1998. Noninvasive two-photon-excitation imaging of tryptophan distribution in highly scattering biological tissues. Optic Commun 154:383–389.

Guo Y, Savage HE, Liu F, Schantz SP, Ho PP, Alfano RR. 1999. Subsurface tumor progression investigated by noninvasive optical second harmonic tomography. Proc Natl Acad Sci USA 96:10854–10856.

Hellwarth R, Christensen P. 1975. Nonlinear optical microscope using second harmonic generation. Appl Opt 14:247–248.

Kirkpatrick ND, Brewer MA, Utzinger U. 2007. Endogenous optical biomarkers of ovarian cancer evaluated with multiphoton microscopy. Cancer Epidemiol Biomarkers Prev 16:2048–2057.

König K, So PTC, Mantulin WW, Tromberg BJ, Gratton E. 1996. Two-photon excited lifetime imaging of autofluorescence in cells during UVA and NIR photostress. J Microsc 183:197–204.

Mazza D, Bianchini P, Caorsi V, Cella F, Mondal PP, Ronzitti E, Testa I, Vicidomini G, Diaspro A. 2008. Non-linear microscopy. In: Pavesi L, Fauchet PM, editors. Biological and medical physics, biomedical engineering. Biophotonics. Berlin: Springer, pp. 47–66.

Millard AC, Wiseman PW, Fittinghoff DN, Wilson KR, Squier JA, Müller M. 1999. Third-harmonic generation microscopy by use of a compact femtosecond fiber laser source. Appl Opt 38:7393–7397.

Millard AC, Campagnola PJ, Mohler W, Lewis A, Loew LM. 2003.Biophotonics, Part B: Methods in enzymology. New York, Washington, DC: Academic Press. Vol. 361, pp.47–69.

Mizutani G, Sonoda Y, Sano H, Sakamoto M, Takahashi T, Ushioda S. 2000. Detection of starch granules in a living plant by optical second harmonic microscopy. J Lumin 87:824–826.

Moreaux L, Sandre O, Blanchard-Desce M, Mertz J. 2000. Membrane imaging by simultaneous second-harmonic generation and two-photon microscopy. Opt Lett 25:320–322.

Muller M, Squier J, Wilson KR, Brakenhoff GJ. 1998. 3D microscopy of transparent objects using third harmonic generation. J Microsc-Oxford 191:266–274.

Nadiarnykh O, LaComb RB, Brewer MA, Campagnola PJ. 2010. Alterations of the extracellular matrix in ovarian cancer studied by second harmonic generation imaging microscopy. BMC Cancer 10:1–14.

Prent N, Green C, Greenhalgh C, Cisek R, Major A, Stewart B, Barzda V. 2008. Intermyofilament dynamics of myocytes revealed by second harmonic generation microscopy. J Biomed Opt 13:041318.

Provenzano PP, Eliceiri KW, Keely PJ. 2009. Multiphoton microscopy and fluorescence lifetime imaging microscopy (FLIM) to monitor metastasis and the tumor microenvironment. Clin Exp Metastasis 26:357–370.

Skala MC, Riching KM, Bird DK, Gendron-Fitzpatrick A, Eickhoff J, Eliceiri KW, Keely PJ, Ramanujam N. 2007. In vivo multiphoton fluorescence lifetime imaging of protein-bound and free nicotinamide adenine dinucleotide in normal and precancerous epithelia. J Biomed Opt 12:024014.

Squier J, Muller M, Brakenhoff G, Wilson KR. 1998. Third harmonic generation microscopy. Opt Express 3:315–324.

Sun CK. 2005. Higher harmonic generation microscopy. Adv. Biochem Eng/Biotechnol 95:17–56.

Sun CK, Chu SW, Chen SY, Tsai TH, Liu TM, Lin CY, Tsai HJ. 2004. Higher harmonic generation microscopy for developmental biology. J Struct Biol 147:19–30.

Tuer A, Tokarz D, Prent N, Cisek R, Alami J, Dumont DJ, Bakueva L, Rowlands J, Barzda V. 2010. Nonlinear multicontrast microscopy of hematoxylin-and-eosin-stained histological sections. J Biomed Opt 15:026018.

Williams RM, Flesken-Nikitin A, Ellenson LH, Connolly DC, Hamilton TC, Nikitin AY, Zipfel WR. 2010. Strategies for high resolution imaging of epithelial ovarian cancer by laparoscopic nonlinear microscopy. Transl Oncol 3:181–194.

Yelin D, Oron D, Korkotian E, Segal M, Silberberg Y. 2002. Third-harmonic microscopy with a titanium sapphire laser. Appl Phys B-Lasers O 74:S97–S101.

Yu W, So PTC, French T, Gratton E. 1996. Fluorescence generalized polarization of cell membranes: a two-photon scanning microscopy approach. Biophys J 70:626–636.

Zoumi A, Yeh A, Tromberg BJ. 2002. Imaging cells and extracellular matrix in vivo by using second-harmonic generation and two-photon excited fluorescence. Proc Natl Acad Sci USA 99: 11014–11019.